Main Manuscript for

Piperine activates the thick filament of resting rat skeletal muscle, enhancing dynamic contractility in a fiber-type-dependent manner

Daniel Z. Kruse [a], Jon Herskind [b], Michel N. Kuehn [c], Annika J. Klotz [c], Anthony L. Hessel [c d], and Kristian Overgaard [a*]

[a] Department of Public Health, Research Unit of Exercise Biology, Aarhus University, Aarhus C 8000, Denmark

[b] Department of Biomedicine, Aarhus University, Aarhus C 8000, Denmark

[c] Institute of Physiology II, University of Muenster, Muenster 48149, Germany

[d] Accelerated Muscle Biotechnologies, Boston, Massachusetts, USA

*** Corresponding author:** Kristian Overgaard

Address: Dalgas Avenue 4, 8000 Aarhus C, Denmark

Email: Overgaard@ph.au.dk

Phone: +4551666548

Author Contributions: D.Z.K., K.O., and A.L.H. conceived the experiments, and D.Z.K., K.O., J.H., M.N.K., A.J.K., and A.L.H. carried them out. D.Z.K. and A.L.H. analyzed data. All authors contributed to the interpretation of the results. D.Z.K. wrote the first draft, and all authors helped shape the paper.

Competing Interest Statement: A.L.H. and M.N.K. are owners of Accelerated Muscle Biotechnologies (AMB). The author team has no competing interests to declare.

Classification: Biological Sciences, Physiology

Keywords: Mammalian Skeletal Muscle, Piperine, Thick-filament regulation, Force-velocity curve, Muscle power

This PDF file includes:

Main Text
Figures 1 to 6
Tables

Abstract

Thick-filament activation, whereby myosin heads transition from an OFF to an ON state, is a key regulatory step in muscle contraction and a promising therapeutic target. The availability of ON-state myosin heads governs dynamic muscle contractility, which is critical to physical function and well-being. Thus, compounds that induce thick-filament activation in skeletal muscle are warranted to explore this therapeutic potential. Piperine, an alkaloid from black pepper, binds to myosin and increases isometric force at submaximal activation levels in both fast and slow-twitch skeletal muscle. The mechanism underlying this effect remains unclear, but may involve thick-filament activation, as shown in cardiac muscle. During contraction, myosin heads naturally shift from the OFF to the ON state, but the kinetics and extent of this transition are fiber-type dependent. Therefore, it remains to be clarified how piperine affects dynamic contractions in fast- and slow-twitch skeletal muscles. We addressed these gaps using fiber small-angle X-ray diffraction and intact-muscle ex vivo contractility experiments on rat extensor digitorum longus (fast-twitch) and soleus (slow-twitch) muscles. X-ray diffraction data suggest that piperine promotes an OFF-to-ON transition of myosin in resting skeletal muscle, increasing the pool of myosin heads available for force generation. Functionally, piperine-induced thick-filament activation substantially enhanced dynamic contractility in both muscle types, with greater improvements in slow-twitch versus fast-twitch muscle under conditions of maximal activation. These findings establish piperine as a tool to probe thick-filament activation in skeletal muscle and guide future studies toward fiber-type–specific effects on recruitment of the contractile reserve capacity.

Significance Statement

Targeting myosin, a key motor protein in muscle, to restore muscle function has become a major focus in muscle physiology. Yet no approved therapies exist for skeletal muscle, making the

identification of compounds with myosin-activating properties a research priority. Skeletal muscles come in two main types: slow (postural) and fast (powerful). Here, we investigated piperine, a natural compound from black pepper, and found that it activates myosin in resting skeletal muscles, making muscles more readily activated. These molecular effects translated into substantial muscle-type-dependent increases in the muscles' ability to recruit their contractile reserve capacity during complex contractions. Our findings propose piperine as a tool for investigating fundamental questions of muscle contraction and the therapeutic opportunities of myosin-activation in skeletal muscle.

Main Text

Introduction

Recent advances in muscle physiology have highlighted the myosin-containing thick filament as an important regulator of muscle contractility (1-3). Therefore, the thick filament also serves as a novel therapeutic target for restoring contractile impairments in cardiac and skeletal muscle (4, 5). In this perspective, modulation of dynamic muscle function is of particular interest, as it is paramount to physical functioning and well-being (6). Resting myosin heads exist in a dynamic equilibrium between the so-called ON and OFF structural states. ON myosin heads are located near actin and are available for interaction, whereas OFF heads are tightly ordered near or within the helical tacks of the thick filament backbone (7). These structural states of myosin in relaxed muscle have previously been shown to regulate dynamic muscle function during contraction via modulating the propensity of each myosin to form crossbridges and thus impact performance (8). While pharmacological small-molecules are proving to be promising thick-filament modulators in treating contractile impairments in cardiomyopathies (5, 9, 10), there is a lack of molecules specifically designed to target skeletal muscle.

A potential tool for investigating thick-filament activation in skeletal muscle is the compound piperine, a natural alkaloid found in black pepper (11, 12). Piperine has been shown to bind to the myosin regulatory light chain (MRLC) (12, 13), a domain known to regulate muscle contractility (14). Using intact rat muscles, Herskind et al. 2024 (15) demonstrated that piperine increases isometric twitch force and force of unfused isometric contractions in both fast- and slow-twitch skeletal muscles. Further**,** piperine increased myofibrillar Ca^{2+} sensitivity, a fundamental property of muscle contraction, in both fiber types without altering resting or contraction-induced sarcoplasmic Ca^{2+} release (15). Interestingly, piperine also enhances Ca^{2+} sensitivity in cardiomyocytes (16), and this effect was ascribed to an increase in ON myosin (17). Together, these studies suggest that piperine has a myosin-mediated contractile effect, which is shared by both cardiac and skeletal muscle, possibly through a constitutively expressed region of myosins across isoforms; however, mechanistic explanations remain speculative.

Dynamic muscle performance in intact muscle can be described by the force–velocity (FV) curve (18), and parameters of the curve can be exploited to study contraction mechanisms. An important molecular modulator of the FV curve is the availability and proportion of ON myosin heads that are ready to engage in crossbridge formation at different external loads (1, 3, 8, 19, 20). During contraction, an OFF-to-ON transition of myosin heads naturally occurs, with the speed and degree of this transition being fiber-type dependent (3, 21-23). Hence, the contractile reserve capacity seems to differ between fiber types during normal contraction. Expanding on this, it is unknown if an increased proportion of ON myosin heads in resting skeletal muscle leads to fiber-type-dependent changes in dynamic contractility. Answering these unknowns is essential to address the therapeutic potential of thick-filament activation in the treatment of debilitating myopathies (24-26). Accordingly, the present study tests the hypothesis that piperine promotes structural thick-filament activation in resting fast- and slow-twitch rat skeletal muscle and investigates whether piperine could enhance power in dynamic contractions. We report that

piperine increases the proportion of ON myosin in resting skeletal muscle of both fiber types, as well as markedly enhancing dynamic contractility in submaximally and maximally activated intact fast and slow muscle in a fiber-type specific manner. This pharmacologically induced thick-filament activation highlights an unused potential of skeletal-muscle therapeutics.

Results

Piperine increases the thick filament activation state in resting slow and fast fiber types

We first determined the effects of piperine on resting thick-filament structure by performing small-angle X-ray diffraction (MyoXRD) experiments (Fig. 1A). MyoXRD was performed at 27°C on permeabilized EDL and soleus fiber bundles. Bundles were mounted at a sarcomere length (SL) of 2.7 µm, corresponding to the optimal length of force production (L_o) (21). Diffraction patterns were collected before and after 20 min incubation in piperine (50 µM) (15, 17).

Fast-twitch fibers. — The equatorial intensity ratio ($I_{1.1}/I_{1.0}$) arises from the mass distribution between the thin ($I_{1.1}$) and thick ($I_{1.0}$) filaments. Piperine increased $I_{1.1}/I_{1.0}$ in fast-twitch EDL fibers compared to baseline (0.58 ± 0.21 (mean ± SD) vs. 0.94 ± 0.55 a.u., P = 0.002) (Fig. 1B), indicating a mass movement (i.e., myosin heads) from the thick filaments towards the thin filaments. The spacing and intensity of the meridional M3 reflection (S_{M3} and I_{M3}) primarily arise from the average distance and general ordering, respectively, of consecutive myosin heads along the thick filament. Hence, increased spacing and less intensity of the M3 are interpreted as an increased proportion of ON myosin heads (7). Surprisingly, the S_{M3} (Fig. 1C) and I_{M3} (Fig. 1D) did not change significantly (S_{M3}: 14.39 ± 0.03 vs. 14.42 ± 0.04 nm, P = 0.139; I_{M3}: 605 ± 166 vs. 536 ± 180 a.u., P = 0.208) in response to piperine. Importantly, the regulatory protein of myosin-binding protein C (MyBP-C) has recently been shown to make a significant contribution to the M3 reflection (27). This is caused by the 3rd order of the ~43 nm MyBP-C periodicity, which overlays the ~14.35 nm first order crown repeat, possibly hiding or exaggerating changes in myosin-head

ordering on the thick filament backbone (27). The spacing of the meridional M6 reflection (S_{M6}) primarily arises from the distance between the repeats of folded-back myosin heads, with minor contributions from other structures within the thick filament (27, 28). The S_{M6} (Fig. 1E) increased slightly in response to piperine (7.23 ± 0.01 vs. 7.24 ± 0.01 nm, P = 0.016), indicative of myosin heads leaving their anchored position on the thick filament. The inter-thick-filament lattice spacing (d_{10}; Fig. 1F) relates to the compression of the sarcomere and was unaffected by piperine (39.9 ± 2.3 vs. 39.2 ± 1.8 nm, P = 0.964). Finally, the intensity of the first-order myosin-layer line (I_{MLL1}), another marker of thick-filament activation, arising from the helical repeat of myosin crowns (27, 28), indicates myosin head ON/OFF states. The I_{MLL1} decreased after piperine incubation, supporting decreased ordering of myosin heads (I_{MLL1}: 1663 ± 716 vs. 999 ± 523 a.u., P = 0.181; Table S1). In summary, our data indicate that piperine induced activation of the thick filament in resting fast-twitch EDL fibers (Fig. 1G; Table S1) (20, 29).

Slow-twitch fibers. — The slow-twitch soleus fibers showed similar but more consistent effects of piperine on resting thick-filament structure. In response to piperine, the $I_{1.1}/I_{1.0}$ showed a marked increase (0.56 ± 0.26 vs. 1.31 ± 0.85 a.u., P < 0.001; Fig. 1H), indicating a movement of mass from the thick filament towards the thin filament. Further, piperine increased the S_{M3} (14.40 ± 0.03 vs. 14.43 ± 0.03 nm, P = 0.009; Fig. 1I) and decreased the I_{M3} (495 ± 102 vs. 398 ± 141 a.u., P = 0.019; Fig. 1J), indicating recruitment of myosin heads from their resting position on the thick filament backbone. The S_{M6} showed a non-significant increase (7.23 ± 0.01 vs. 7.24 ± 0.01 nm, P = 0.148; Fig. 1K). Once again, the d_{10} was unaffected by piperine (39.8 ± 2.2 vs. 40.1 ± 1.9 nm, P = 0.070; Fig. 1L), suggesting no effects on sarcomere compression. Finally, the I_{MLL1} decreased markedly in response to piperine (1544 ± 665 vs. 681 ± 190 a.u., P = 0.014; Table S1). Hence, our data consistently show a strong OFF-to-ON transition of the thick filament in the soleus fibers in response to piperine (Fig. 1M; Table S1). Taken together, our data indicate that piperine

activated the thick filament in resting fibers of both types of skeletal muscle, manifesting as an OFF-to-ON signature across the diffraction outcomes.

Whole-muscle contractile experiments demonstrate contraction-type-dependent effects of piperine

From experiments with permeabilized preparations above, we predicted that contraction performance would be altered as well, which we explored in whole muscle. The main experimental protocol was performed using an ex vivo two-chamber contractile setup (Model 305 Dual Muscle Lever, Aurora Scientific, Aurora, ON, Canada) as illustrated in Fig. 2A. This setup allows simultaneous experiments on contralateral muscles (Fig. 2B), in which contraction force and muscle length are measured during electrically induced contractions against varying external loads. To study how piperine would enhance contractile performance, isometric and dynamic muscle function of both muscle types were tested during a 60-min incubation (piperine 50 µM vs. vehicle) (15) surrounded by two force-velocity (FV) tests (FV1-2), respectively (Fig. 2B). After the baseline FV test (FV1) (presented below), contralateral muscles were treated with piperine and vehicle (ethanol 0.1% of buffer volume) in the incubation. During the incubation, isometric twitch, unfused tetani, and fused tetani were induced at regular intervals (Tables S2 and S3). These three isometric contraction types were tested due to their distinct underlying features of intracellular Ca^{2+} release, summation of forces from subsequent action potentials, and thick-filament activation level (1, 3). We report differences between muscles treated with piperine and vehicle, expressed relative to the baseline level.

Fast-twitch muscles. — In EDL muscles, piperine increased twitch (Fig. 3A) and unfused tetanic (Fig. 3B) forces, while not affecting fused tetanic force (Fig. 3C). After 60 min of incubation, piperine increased twitch and unfused force by 36% [29:43] (mean [95%CI]) ($P < 0.001$) and 38% [31:46] ($P < 0.001$), respectively. At the same time, the maximal rate of force development (RFD) (Table S2) of the twitch, unfused, and fused tetanic contractions increased by 34% [28:41] (P <

0.001), 35% [27:43] (P < 0.001), and 2.0% [1.1:2.8] (P < 0.001), respectively. Finally, 60 min of piperine treatment increased the force relaxation time (RT) (Table S2) of the twitch by 3.5% [1.1:5.8] (P < 0.008). In contrast, piperine decreased the RT of unfused contractions by 6.0% [3:9.1] (P < 0.001), while the fused contractions did not show any consistent changes (2.6% [-0.2:5.4], P = 0.144).

Slow-twitch muscles. — Similar to the EDL muscles, the twitch (Fig. 4A) and unfused (Fig. 4B) forces of the soleus muscles increased in response to piperine, while the fused tetanic force was unaffected (Fig. 4C). In the soleus, piperine increased twitch and unfused force by 43% [37:49] (P < 0.001) and 21% [16:27] (P < 0.001), respectively. Twitch and unfused tetanic RFD of the soleus muscles (Table S3) increased by 32% [27:37] (P < 0.001) and 37% [31:42] (P < 0.001), respectively. Notably, RFD of fused tetanic contractions in soleus muscles increased substantially by 16% [13:19] (P < 0.001). Also, piperine increased soleus twitch RT (Table S3) by 5.3% [0.5:10.2] (P < 0.035), decreased unfused tetanic RT by 7.3% [5:9.7] (P < 0.001), and did not show consistent changes in RT of fused contractions. Finally, in an additional incubation phase (Fig. S1), we showed that the effects of piperine were both reversible and reproducible (EDL, Table S2; soleus, Table S3).

Thick-filament activation by piperine enhances low- and high-frequency dynamic muscle function, with more pronounced effects in slow-twitch muscle

Muscles are rarely maximally activated in vivo; therefore, a comprehensive assessment of muscle function must also include testing at submaximal activation levels. Accordingly, FV curves were determined (denoted as FV1-2 in Fig. 2B) at both submaximal and maximal activation levels by fiber-type-specific low- and high-frequency stimulation protocols (EDL: 60/150 Hz; soleus: 20/80 Hz). Below, we show exemplary contractions (Fig. 5A) along with FV curves and power curves from baseline (FV1) testing (Fig. 5B and C). We report differences between muscles treated with

piperine and vehicle (FV2) expressed relative to baseline (FV1). Absolute values from FV testing are shown in the SI Appendix, Tables S4 and S5, respectively.

Low-frequency activation. — Piperine induced marked and highly consistent increases in low-frequency dynamic muscle function in both muscle types. In the EDL (Fig. 5D), piperine increased low-frequency V_{max} and P_{max} by 25% [23:28] ($P < 0.001$) and 36% [31:40] ($P < 0.001$), respectively. Also, the curvature of the FV curve increased (a/F_o decreased) by 36% [27:46] ($P < 0.001$). In the soleus (Fig. 5E), piperine increased low-frequency V_{max} and P_{max} by 20% [12:28] ($P = 0.005$) and 54% [46:62] ($P < 0.001$), respectively, with no effect on curvature ($P = 0.277$).

High-frequency activation. — Interestingly, piperine also showed effects on the high-frequency FV curves in both muscle types. In the EDL (Fig. 5F), piperine increased V_{max} by 5.5% [2.6:8.3] ($P = 0.001$) and increased curvature (a/F_o decreased) by 13% [4:22] ($P = 0.013$), while not affecting P_{max} ($P = 0.318$). In contrast, the soleus muscles (Fig. 5G) exclusively showed positive effects in response to piperine, as V_{max} and P_{max} increased by respectively 9% [6:12] ($P = 0.001$) and 11% [7:14] ($P = 0.002$) without affecting curvature ($P = 0.131$). Finally, in an additional FV test (FV3) (Fig. S1), the effects of piperine on dynamic muscle function were shown to be both reversible and reproducible (Tables S4 and S5).

Piperine selectively increases the rate of crossbridge cycling in fast-twitch EDL muscle

As a separate experiment, we determined the effects of piperine (versus vehicle) on the rate of actomyosin crossbridge cycling at L_o in EDL and soleus muscles. Experiments were performed using the same setup and incubations (60 min) as described in Fig. 2A and B. We measured the rate constant of isometric tension redevelopment (K_{tr}) after imposing muscles unloaded shortening and a fast restretch back to L_o (EDL force trace is shown in Fig. 6A and B). We employed fiber-type-dependent stimulation protocols for the K_{tr} determination, which are detailed in the Materials and Methods of the SI Appendix. The approach allows for assessment of

isometric force development under circumstances where 1) intracellular calcium levels are maximal from the beginning due to continuous electrical stimulation, and 2) the number of attached crossbridges at the beginning is minimal due to prior length manipulation of the muscles.

After 60 min of incubation, the potentiating effect of piperine was visible in both muscle types as the twitch force increased as expected (EDL: 27% [17:37]; soleus: 34% [21:47]). In the EDL muscles (Fig. 6C), K_{tr} increased by 15% [7:22] ($P < 0.001$) after 60 min of incubation compared to vehicle treatment. In contrast, K_{tr} of the soleus muscles (Fig. 6D) was unchanged after 60 min of incubation (0.5% [-0.5:1.5], $P = 0.321$). Hence, our data suggest that piperine increases the rate of actomyosin crossbridge cycling in EDL muscles, but not in soleus muscles.

Discussion

Piperine induces thick-filament activation in resting skeletal muscle of both fiber types

The positioning of myosin heads relative to the thick filament governs their availability for actin interaction upon Ca^{2+}-mediated thin-filament activation (1). Hence, to test if the previously observed potentiation of contractile force induced by piperine in both fiber types of skeletal muscle (15) could be caused by activation of the thick filament, we applied MyoXRD on resting permeabilized muscle fibers. Taken together, our MyoXRD data show an OFF-to-ON transition of the thick filament in both fiber types in response to piperine. There was consistent directionality across all parameters pointing to an OFF-to-ON transition; however, not all changes were statistically significant in the EDL bundles. Further, unpaired analyses in EDL bundles supported an OFF-to-ON transition by revealing significant changes ($P < 0.05$) in $I_{1.1/I1.0}$, S_{M3}, and $S_{M6,}$ and borderline significance in I_{M3} ($P = 0.066$) and I_{MLL1} ($P = 0.081$) after removing an outlier from the I_{M3} (outlier > mean + 1.96 × SD). A similar approach in the soleus bundles showed significant effects ($P < 0.05$) on the $I_{1.1}/I_{1.0}$, S_{M3}, I_{M3}, S_{M6}, and I_{MLL1}. Since the directions of these changes were all in line with the classic OFF-to-ON signature (20, 29), we find that our MyoXRD data

clearly support the conclusion that piperine induces thick-filament activation in resting skeletal muscle of both fiber types.

While thick-filament activation patterns during contraction have been subject to multiple studies in recent years (3, 21-23, 30), thick-filament activation in resting skeletal muscles and its consequences for contractility have been very sparsely investigated. At present, options for studying exogenous thick-filament activation in intact skeletal muscles rely on the use of 1) transgenic animals expressing higher-than-normal levels of the thick-filament activating 2-deoxy-ATP (dATP) (31) or 2) cardiac-specific thick-filament activators with poor affinity for especially fast skeletal muscle (24, 25, 32-35). Another approach is the induction of the physiological potentiation phenomenon, post-tetanic potentiation (PTP) (14), which potentiates force in fast-twitch fibers by Ca^{2+}-dependent MRLC phosphorylation. Using time-resolved MyoXRD on live tarantulas, it has been elegantly shown that PTP induces an OFF-to-ON transition of the thick filament, which causes the subsequent force potentiation (36). Yet, PTP is a very short-lived force potentiation in fast skeletal muscles, which only activates the resting thick filament on a timescale of seconds. Thus, these approaches all have limitations in terms of their accessibility, ability to induce thick-filament activation acutely, or to induce activation for longer periods of time in skeletal muscle preparations. Piperine has previously been shown to activate the thick filament in resting cardiomyocytes (17). Our data expand on those findings, showing that piperine also induces thick-filament activation across both fiber types of skeletal muscle. Hence, piperine represents a promising tool compound for inducing thick-filament activation in skeletal muscle, offering advantages over currently limited options such as PTP, dATP, or cardiac-specific activators.

Thick-filament activation by piperine enhances dynamic contractility in skeletal muscles, with more pronounced effects in slow muscles

Dynamic muscle function is essential for physical functioning and well-being (6), making it a highly important outcome to assess when investigating modulation of the contractile machinery. We investigated the effects on dynamic muscle function in fast and slow skeletal muscles by determining FV curves. Here we found that piperine-induced thick-filament activation led to a marked enhancement of V_{max} and P_{max} during low-frequency activation in both muscle types (Fig. 5D and E). These findings correlate well with the findings reported by Herskind et al. 2024 showing that piperine potentiates isometric contractions induced by low-frequency activation (15). Skeletal muscles activated at low frequencies will have sub-saturating intracellular Ca^{2+} levels, and thereby the contractile machinery will be sensitive to the piperine-induced modulation of Ca^{2+}-sensitivity (15). In the present study, the magnitudes of potentiation of P_{max} were substantial (EDL: ~36% and soleus: ~54%), indicating great potential of exogenous thick-filament activation to enhance low-frequency dynamic contractility, which is the most common type of muscle contraction in vivo.

Surprisingly, we also found that piperine enhanced dynamic muscle function during high-frequency muscle activation (Fig. 5F and G). Previous studies have shown that 1) a resting pool of ON myosin motors drives low-load shortening (20) and 2) the number of available myosin motors governs the force-velocity curve (8). Here we show that increasing the resting pool of ON myosin motors 1) increases high-frequency V_{max} (EDL: ~5% and soleus: ~9%) and 2) shifts the overall force-velocity curve of both muscle types towards higher power output during high-frequency activation. In contrast to our findings, it has previously been reported that piperine does not affect the shortening velocity at 25% of maximal isometric force in maximally Ca^{2+}-activated single fibers (12). These experiments were performed using a temperature-jump protocol (5-25ºC) while testing shortening velocity at only one external load (25% of isometric max). Hence, discrepancies between our findings and the previous study may be explained by a more comprehensive assessment of dynamic contractility performed in our study, along with differences in the experimental temperatures. Taken together, piperine seems able to modulate

the underlying physiological determinants of dynamic muscle function, leading to substantial changes in dynamic contractility.

Based on our findings of the thick-filament activation induced by piperine, our contractile experiments can be viewed in a broader perspective. Hence, here we show that exogenous thick-filament activation of skeletal muscles potentiates dynamic muscle function of fast and slow muscles during both low- and high-frequency activation. Interestingly, the potential of piperine to enhance dynamic contractility during high-frequency activation seemed more pronounced in the slow muscles compared to the fast muscles, as P_{max} increased exclusively in the slow soleus muscles (~10.5%). Thus, our data indicate fiber-type-specific differences in the level of enhancement of dynamic muscle function by exogenous thick-filament activation. These differences may be explained by recent findings, showing that the kinetics of thick-filament activation during contraction are fiber type-dependent (21-23). Further, Hill et al. 2025 (3) elegantly showed that not only the kinetics, but also the overall degree of thick-filament activation during isometric fused tetani, is lower in the slow soleus compared to the fast EDL, indicating fiber-type differences in the contractile reserve capacity. In this perspective, we speculate that the large effects on dynamic muscle function in the slow soleus muscle could indicate that piperine elevates the recruitment of the contractile reserve capacity during contraction.

Effects of piperine on force development kinetics suggest complex fiber-type-specific mechanisms

We observed seemingly contradictory effects of piperine on force development (RFD in Tables S2 and 3) and redevelopment kinetics (K_{tr} in Table S6) that reveal the complexity of piperine-potentiation across fiber types. In EDL muscles, piperine increased K_{tr} by ~15% under conditions of maximal Ca^{2+} and a reduced number of attached crossbridges yet increased initial RFD of fused tetanic contractions by only ~2%. Conversely, in soleus muscles, K_{tr} was unchanged while the initial RFD of fused tetani increased by ~16%. In notion, Herskind et al. (15) reported a similar

tendency, with piperine inducing numerically larger increases in fused tetanic RFD of soleus muscles compared to EDL. The divergent findings likely reflect different rate-limiting steps in force development between fiber types and experimental conditions. K_{tr}, measured after unloaded shortening and re-stretch, primarily assesses crossbridge kinetics when thin filaments are fully activated and the number of attached crossbridges is artificially reduced. In contrast, peak RFD during normal tetanic contractions integrates multiple processes, including: 1) Ca^{2+}-dependent thin- and thick-filament activation kinetics, 2) strain-dependent thick-filament activation kinetics, and 3) crossbridge cycling (1, 37). Also, we cannot exclude that these discrepancies may be due to isoform-dependent interactions of piperine with sarcomeric regulatory proteins as MRLC, MyBP-C, and titin. Hence, the cause for these divergent findings may be found in the complex interaction between the effects of piperine and the effects of Ca^{2+}, strain, other sarcomeric proteins, and differences between fiber types. We hypothesize that piperine has an exclusive effect on crossbridge kinetics (detected by K_{tr}) in EDL muscles, which tends to support previous findings of a piperine-induced increase in resting myosin ATPase activity in fast-twitch but not in slow-twitch fibers (12, 38). These changes were seen without substantial changes to peak RFD in EDL, which may already be near-maximal in the fast muscle type. In contrast, in the soleus muscles, piperine-induced thick-filament activation may eliminate a rate-limiting recruitment step of ON myosin during normal contractions, dramatically increasing RFD, while not affecting isolated crossbridge cycling kinetics measured by K_{tr}. However, we acknowledge that these data are exploratory, and interpretation is speculative.

Limitations

In MyoXRD experiments, we used permeabilized resting muscle fibers, a preparation known to experience cell swelling that can lead to some disruption of the resting sarcomere order (39). Cell swelling can be counteracted by applying a compressor molecule such as dextran; yet, due to piperine's poor solubility and the viscosity of dextran, we did not include dextran. However, we

have no reason to believe that the initial cell swelling modifies the effect of piperine (40). Finally, we did not determine the fiber types of the fibers used in MyoXRD experiments; however, we utilized rat EDL and soleus muscles as they are composed of ~90-95% type II and I fibers, respectively (41).

Intact ex vivo muscle preparations have a limited durability of 8-9 hours in our experimental setup. In our contractile experiments, we had to apply long incubation phases to reach plateaus in force potentiation (15). Further, FV tests were executed throughout 60 min, making the overall experimental protocol strenuous on the preparations. We handled these issues by determining neighboring FV points at different points in the sequence to average the potential impacts of incubation time and fatigue during the FV test (42). The experimental approach and setup we applied to investigate crossbridge cycling rates K_{tr} in intact EDL and soleus muscles have previously been used by Kristensen et al. (42, 43). In these studies, Kristensen et al. demonstrated that the method was sensitive to changes in K_{tr} imposed by fatigue and physiologically induced potentiation. We cannot discriminate between attachment and detachment rates by this method; therefore, we used this approach as an explorative outcome.

Future directions

We observed marked fiber-type-dependent differences in the potential of piperine to enhance dynamic contractility. This may suggest that thick-filament activation modifies the natural contraction-induced activation kinetics of the thick filament in a fiber-type-dependent manner. Hence, future studies should utilize time-resolved MyoXRD to understand the nature of the fiber-dependent effects of exogenous thick-filament activation on dynamic muscle function. Such information will be fundamental to determining the therapeutic potential of pharmacological skeletal-muscle thick-filament activation to mitigate contractile impairments.

Conclusion

To conclude, our data strongly indicate that piperine 1) induces thick-filament activation in resting skeletal muscle of both fiber types, and 2) enhances dynamic muscle function at submaximal and maximal activation levels in both fast and slow skeletal muscles. Hence, we propose piperine as a tool compound for the investigation of exogenous thick-filament activation in skeletal muscle. Further, we reveal that thick-filament activation in skeletal muscle leads to fiber-type-dependent magnitudes of potentiation of dynamic muscle function. Such effects must be further investigated and must be accounted for in future efforts to leverage the therapeutic potential of skeletal-muscle thick-filament activation in the treatment of contractile impairments.

Materials and Methods

Muscle preparations

Intact extensor digitorum longus (EDL) and soleus muscles were dissected from 4-week-old female Wistar rats (Janvier Labs, LeGenest-Saint-Isle, France). EDL and soleus muscles were used because of their vastly different fiber type distributions (EDL ~90% type II fibers and soleus ~90% type I fibers) (41). Glycerol-permeabilized bundles of fibers were used for the determination of resting thick-filament structure (40), and intact muscles were used for contractile experiments (described in the Materials and Methods in the SI Appendix).

Assessment of resting thick-filament structure using small-angle X-ray diffraction

Resting thick-filament structure was determined in the absence and presence of piperine in permeabilized bundles of EDL and soleus fibers. After permeabilization, muscles were stored 2-4 weeks at -20ºC, before being transferred to the experimental facility on ice. On the experimental

day, muscles were vigorously washed in cold relaxing solution (concentrations in mM: Potassium propionate 91.2, $MgCl_2$ 3.6, Na_2-ATP 2.5, EGTA 7.0, Imidazole 20.0, and Halt™ protease inhibitor cocktail 1% [Thermo Fisher Scientific, Waltham, MA, USA], pH 7.0 at room temperature) to remove glycerol. Then, 2-6 mm long bundles of ~5-15 muscle fibers were dissected (EDL: 28 bundles, 7 animals; soleus: 20 bundles, 6 animals), and silk suture knots (sizing 5-0) were tied at both ends. Finally, bundles were mounted onto a specially designed muscle mechanics rig for MyoXRD, described elsewhere (44).

MyoXRD was conducted at the P03 / MiNaXS beamline (Petra III, DESY, Hamburg); comprehensive technical specifications and image analysis procedures are described in the Materials and Methods of the SI Appendix. Bundles were manually aligned and targeted with the X-ray beam using an inline camera. This camera also allowed for visual control of the quality of samples during experiments. For each condition, the beam scanned the sample along its long length to produce ~25-50 images with 100 ms exposure per image at a speed where no part of the sample was exposed to more than 300 ms of radiation in total, which in pilot studies produced negligible radiation damage. Line scans were separated by 50 µm displacements along the axis perpendicular to the long axis of the sample. A subgroup of EDL bundles (n = 9) was tested at SL 2.4 and 2.7 µm before and after piperine incubation, using a passive ramp-hold protocol as previously described (discussed in the Materials and Methods of the SI Appendix) (45).

Experimental setup and solutions used in contractile experiments

Immediately after dissection, intact muscles were mounted in oxygenated chambers (constant perfusion with 95% O_2 and 5% CO_2). Chambers were filled with 100 ml of standard Krebs-Ringer (KR) buffer at 30°C (concentrations in mM: NaCl 122.13, KCl 2.84, $CaCl_2$ 1.27, $MgSO_4$ 1.19, KH_2PO_4 1.19, and $NaHCO_3$ 25.06) (pH 7.2-7.4 at room temperature). After mounting in chambers, muscles were stimulated to elicit a brief isometric tetanus to test the integrity of the knots, and

then they rested for 30 min. The length of optimal isometric force production (L_o) was determined using triplet stimulation, and then the muscles rested for 20 min before the experiments began. Isometric and dynamic muscle contractions were evoked by electrical stimulation (described in the SI Appendix along with analysis of contractile outcomes) against a computer-controlled lever arm imposing various external loads (DMC 5.500, Aurora Scientific). Piperine (Sigma-Aldrich, St Louis, MO, USA; cat.no. P49007) was dissolved in ethanol 96%. In the final buffers, the piperine concentration was 50 µM with ethanol (vehicle treatment) making up 0.1% of the total buffer volume.

Assessment of low- and high-frequency dynamic muscle function during FV testing

Isotonic FV curves were determined by using the afterload method, as previously described (42, 46). Each FV curve was determined by measuring the maximal shortening velocity (mm/s) against seven external load levels (in this order: 15, 80, 27.5, 40, 5, 100, and 60% of maximal unfused- and fused-tetanic isometric force). The exact protocols are described in the SI Appendix and illustrated in Fig. S2. From measured force and shortening-velocity values, FV curves were fitted (mean $R^2 > 0.98$) using Hill's force equation (1), and the corresponding power curves (force × velocity) were fitted using Hill's power equation (2):

$$(1)\quad F = \frac{F_o \cdot b - a \cdot V}{b + V}$$

$$(2)\quad P = \frac{F_o \cdot b - a \cdot V}{b + V} \cdot V$$

In the above equations, F_o is the measured maximal isometric force, V is the shortening velocity, and a and b are constants. The maximal unloaded shortening velocity (V_{max}) (mm/s) and maximal isometric force production (F_{max}) (mN) were estimated from the extrapolation of these curves.

Likewise, the curvature of the FV curve (a/F_o) (a.u.) and the maximal power production (P_{max}) (J/s) were estimated.

Assessment of the overall rate of crossbridge cycling

K_{tr} was used to assess the overall crossbridge cycling rate under maximal Ca^{2+} conditions in intact rat muscles. It was experimentally determined in both muscle types as previously described (42). The exact protocols and curve-fitting procedures are described in the Materials and Methods of the SI Appendix.

Statistical analysis

Descriptive values are presented as mean ± standard deviation (SD), while differences (absolute and percentage) are presented as mean difference followed by a 95% confidence interval. A significance level of 0.05 was used, and all statistical analyses and figures were made using GraphPad Prism 10.2. Data were assessed for normality by visual inspection of quantile-quantile (QQ) plots, and assumptions of equal standard deviations were tested by F-tests. To meet assumptions of normality, some MyoXRD outcomes (EDL: $I_{1.1}/I_{1.0}$, S_{M3}, and I_{M3}; soleus: $I_{1.1}/I_{1.0}$) were log-transformed for statistical analysis. Parametric statistical methods were used, and when appropriate, post hoc tests were applied; exact approaches are described in the figure legends.

Acknowledgments

We thank Khoi Nguyen from Accelerated Muscle Biotechnologies (AMB) for his assistance in the MyoXRD experiments. Also, we thank Cuno Rasmussen for his assistance in designing software for the analysis of the contractile data. We acknowledge DESY (Hamburg, Germany), a member of the Helmholtz Association HGF, for the provision of experimental facilities. Parts of this

research were carried out at Petra III. Data was collected using the P03 beamline 18ID operated/provided by DESY Photon Science. We would like to thank Matthias Schwartzkopf and Jan Rubeck for assistance during the experiments. Beamtime was allocated for proposals I-20221421 and II-20241178. The study was supported by grants from the Research Pool of the Ministry of Culture in Denmark (SUAKPKfor2W.2024-022) and Aarhus University Research Foundation (AUFF-E-2023-9-11).

References

1. E. Brunello, L. Fusi, Regulating Striated Muscle Contraction: Through Thick and Thin. *Annual Review of Physiology* **86**, 255–275 (2024).
2. M. Irving, Regulation of Contraction by the Thick Filaments in Skeletal Muscle. *Biophys J* **113**, 2579–2594 (2017).
3. C. Hill *et al.*, Distinct distributions of myosin motor conformations during contraction of slow and fast skeletal muscle. *bioRxiv* 10.1101/2025.10.13.679501, 2025.2010.2013.679501 (2025).
4. W. J. Claassen, R. J. Baelde, R. A. Galli, J. M. de Winter, C. A. C. Ottenheijm, Small molecule drugs to improve sarcomere function in those with acquired and inherited myopathies. *Am J Physiol Cell Physiol* **325**, C60–c68 (2023).
5. S. J. Lehman, C. Crocini, L. A. Leinwand, Targeting the sarcomere in inherited cardiomyopathies. *Nat Rev Cardiol* **19**, 353–363 (2022).
6. S. R. Freitas, C. Cruz-Montecinos, S. Ratel, R. S. Pinto, Powerpenia Should be Considered a Biomarker of Healthy Aging. *Sports Med Open* **10**, 27 (2024).
7. W. Ma, T. C. Irving, Small Angle X-ray Diffraction as a Tool for Structural Characterization of Muscle Disease. *Int J Mol Sci* **23** (2022).
8. G. Piazzesi *et al.*, Skeletal muscle performance determined by modulation of number of myosin motors rather than motor force or stroke size. *Cell* **131**, 784–795 (2007).
9. I. Olivotto *et al.*, Mavacamten for treatment of symptomatic obstructive hypertrophic cardiomyopathy (EXPLORER-HCM): a randomised, double-blind, placebo-controlled, phase 3 trial. *Lancet* **396**, 759–769 (2020).
10. A. A. Voors *et al.*, Effects of danicamtiv, a novel cardiac myosin activator, in heart failure with reduced ejection fraction: experimental data and clinical results from a phase 2a trial. *Eur J Heart Fail* **22**, 1649–1658 (2020).
11. C. T. A. Lewis *et al.*, Dysregulated skeletal muscle myosin super-relaxation and energetics in male participants with type 2 diabetes mellitus. *Diabetologia* 10.1007/s00125-025-06436-0 (2025).
12. L. Nogara *et al.*, Piperine's mitigation of obesity and diabetes can be explained by its up-regulation of the metabolic rate of resting muscle. *Proc Natl Acad Sci U S A* **113**, 13009–13014 (2016).

501 13. D. Tolkatchev *et al.*, Piperine, an alkaloid inhibiting the super-relaxed state of myosin,
502 binds to the myosin regulatory light chain. *Arch Biochem Biophys* **659**, 75–84 (2018).
503 14. R. Vandenboom, Modulation of Skeletal Muscle Contraction by Myosin Phosphorylation.
504 *Compr Physiol* **7**, 171–212 (2016).
505 15. J. Herskind, N. Ørtenblad, A. J. Cheng, P. Pedersen, K. Overgaard, Piperine enhances
506 contractile force in slow- and fast-twitch muscle. *J Physiol* **602**, 2807–2822 (2024).
507 16. V. P. Jani, W. Ma, Thick-Filament-Based Regulation and the Determinants of Force
508 Generation. *Biomedicines* **13**, 703 (2025).
509 17. V. P. Jani *et al.*, The structural OFF and ON states of myosin can be decoupled from the
510 biochemical super- and disordered-relaxed states. *PNAS Nexus* **3**, pgae039 (2024).
511 18. J. Alcazar, R. Csapo, I. Ara, L. M. Alegre, On the Shape of the Force-Velocity Relationship
512 in Skeletal Muscles: The Linear, the Hyperbolic, and the Double-Hyperbolic. *Front*
513 *Physiol* **10**, 769 (2019).
514 19. L. Fusi *et al.*, Minimum number of myosin motors accounting for shortening velocity
515 under zero load in skeletal muscle. *J Physiol* **595**, 1127–1142 (2017).
516 20. M. Linari *et al.*, Force generation by skeletal muscle is controlled by mechanosensing in
517 myosin filaments. *Nature* **528**, 276–279 (2015).
518 21. H. M. Gong, W. Ma, M. Regnier, T. C. Irving, Thick filament activation is different in fast-
519 and slow-twitch skeletal muscle. *The Journal of Physiology* **600**, 5247–5266 (2022).
520 22. J. Zhao, L. Qi, S. Yuan, T. C. Irving, W. Ma, Differences in thick filament activation in fast
521 rodent skeletal muscle and slow porcine cardiac muscle. *The Journal of Physiology* **602**,
522 2751–2762 (2024).
523 23. C. Hill, E. Brunello, L. Fusi, J. G. Ovejero, M. Irving, Activation of the myosin motors in
524 fast-twitch muscle of the mouse is controlled by mechano-sensing in the myosin
525 filaments. *J Physiol* **600**, 3983–4000 (2022).
526 24. J. Lindqvist, E. J. Lee, E. Karimi, J. Kolb, H. Granzier, Omecamtiv mecarbil lowers the
527 contractile deficit in a mouse model of nebulin-based nemaline myopathy. *PLoS One* **14**,
528 e0224467 (2019).
529 25. E. Karimi *et al.*, Characterization of NEB pathogenic variants in patients reveals novel
530 nemaline myopathy disease mechanisms and omecamtiv mecarbil force effects. *Acta*
531 *Neuropathol* **147**, 72 (2024).
532 26. J. Ochala, P. J. Radell, L. I. Eriksson, L. Larsson, EMD 57033 partially reverses ventilator-
533 induced diaphragm muscle fibre calcium desensitisation. *Pflugers Arch* **459**, 475–483
534 (2010).
535 27. N. A. Koubassova *et al.*, Annotating the x-ray diffraction pattern of vertebrate striated
536 muscle. *Biophys J* 10.1016/j.bpj.2025.09.019 (2025).
537 28. A. L. Hessel, Milestone for the interpretation of muscle X-ray diffraction patterns.
538 *Biophys J* 10.1016/j.bpj.2025.09.046 (2025).
539 29. W. Ma *et al.*, The Super-Relaxed State and Length Dependent Activation in Porcine
540 Myocardium. *Circ Res* **129**, 617–630 (2021).
541 30. C. Hill, E. Brunello, L. Fusi, J. G. Ovejero, M. Irving, Myosin-based regulation of twitch
542 and tetanic contractions in mammalian skeletal muscle. *eLife* **10**, e68211 (2021).
543 31. W. Ma *et al.*, Myosin dynamics during relaxation in mouse soleus muscle and
544 modulation by 2'-deoxy-ATP. *J Physiol* **598**, 5165–5182 (2020).

32. L. Nagy *et al.*, The novel cardiac myosin activator omecamtiv mecarbil increases the calcium sensitivity of force production in isolated cardiomyocytes and skeletal muscle fibres of the rat. *Br J Pharmacol* **172**, 4506–4518 (2015).
33. S. Governali *et al.*, Orthophosphate increases the efficiency of slow muscle-myosin isoform in the presence of omecamtiv mecarbil. *Nat Commun* **11**, 3405 (2020).
34. I. K. Potoskueva *et al.*, The effect of omecamtiv mecarbil on actin-myosin interaction in the disused rat soleus muscle. *Arch Biochem Biophys* **769**, 110442 (2025).
35. M. B. Radke *et al.*, Small molecule-mediated refolding and activation of myosin motor function. *Elife* **3**, e01603 (2014).
36. R. Padrón *et al.*, The myosin interacting-heads motif present in live tarantula muscle explains tetanic and posttetanic phosphorylation mechanisms. *Proc Natl Acad Sci U S A* **117**, 11865–11874 (2020).
37. M. Caremani *et al.*, Dependence of myosin filament structure on intracellular calcium concentration in skeletal muscle. *J Gen Physiol* **155** (2023).
38. M. Montesel *et al.*, A combined experimental and computational analysis of mantATP turnover in skinned muscle fibers. *Proc Natl Acad Sci U S A* **122**, e2502652122 (2025).
39. M. Caremani *et al.*, Dependence of thick filament structure in relaxed mammalian skeletal muscle on temperature and interfilament spacing. *J Gen Physiol* **153** (2021).
40. A. L. Hessel *et al.*, The distinctive mechanical and structural signatures of residual force enhancement in myofibers. *Proc Natl Acad Sci U S A* **121**, e2413883121 (2024).
41. A. S. Cornachione, P. C. Benedini-Elias, J. C. Polizello, L. C. Carvalho, A. C. Mattiello-Sverzut, Characterization of fiber types in different muscles of the hindlimb in female weanling and adult Wistar rats. *Acta Histochem Cytochem* **44**, 43–50 (2011).
42. A. M. Kristensen, O. B. Nielsen, T. H. Pedersen, K. Overgaard, Fatiguing stimulation increases curvature of the force-velocity relationship in isolated fast-twitch and slow-twitch rat muscles. *J Exp Biol* **222** (2019).
43. A. M. Kristensen, O. B. Nielsen, K. Overgaard, Effects of manipulating tetanic calcium on the curvature of the force-velocity relationship in isolated rat soleus muscles. *Acta Physiol (Oxf)* **222** (2018).
44. A. L. Hessel *et al.*, Titin force in muscle cells alters lattice order, thick and thin filament protein formation. *Proceedings of the National Academy of Sciences* **119**, e2209441119 (2022).
45. A. L. Hessel *et al.*, Myosin-binding protein C regulates the sarcomere lattice and stabilizes the OFF states of myosin heads. *Nature Communications* **15**, 2628 (2024).
46. A. M. Kristensen, K. B. MacDougall, B. R. MacIntosh, K. Overgaard, Is curvature of the force-velocity relationship affected by oxygen availability? Evidence from studies in ex vivo and in situ rat muscles. *Pflugers Arch* **472**, 597–608 (2020).
47. J. Herskind (2022) PhD dissertation - Evaluation of low-frequency fatigue in dynamic contractions and potentiation of low-frequency force. in *Department of Public Health* (Aarhus University), p 132.

Figure legends

Figure 1. Effects of 50 µM piperine on resting sarcomere structure of bundles of fast (extensor digitorum longus, EDL) and slow (soleus) rat skeletal muscles. (A) Representative X-ray diffraction pattern from one soleus bundle with reflections originating from longitudinally (meridional) and transversely (equatorial) repeating structures. On the representative image, it is stated whether the intensity and/or spacing of the reflection was extracted. Further, an illustration of the sarcomeric structures from which the diffractions arise is shown. Red arrows show the primary origin of the reflection, and dotted lines indicate that multiple structures contribute to the reflection. We report baseline (black circles) and piperine (green circles) values from individual bundles (with lines connecting repeated measurements from the same bundle) and group means ± SEM (blue lines with error bars). For the EDL (B, C, D, E, and F) and soleus (H, I, J, K, and L) bundles, the following outcomes were extracted. (B and H) The equatorial intensity ratio ($I_{1.1}$ / $I_{1.0}$). (C and I) The spacing of the M3 reflection (S_{M3}), and (D and J), the intensity of the M3 reflection (I_{M3}). (E and K) The spacing of the M6 reflection (S_{M6}). (F and L) The inter-thick-filament lattice spacing (d_{10}) (illustrated in the top-right corner (45)). (G and M) Illustrations of our interpretation of the changes induced by piperine in the fast and slow fibers, respectively. Vertical arrows indicate that the change was statistically significant, and vertical arrows in parentheses indicate the numerical direction of non-significant findings. Data from EDL bundles (n = 9-21 bundles) and soleus bundles (n = 11-14 bundles) were analyzed for the effect of treatment (baseline vs. piperine) using repeated measures ANOVAs (significance level: $P < 0.05$).

Figure 2. Experimental setup and protocol for whole-muscle contractility experiments investigating the effects of piperine (50 µM) and vehicle treatment on isometric and dynamic muscle function. (A) Intact fast (extensor digitorum longus, EDL) or slow-twitch (soleus) skeletal muscles from 4-week-old rats were dissected and mounted in the setup illustrated in the top-left corner. Muscles were mounted at the optimal length for force production (L_o) in temperature-controlled (30°C) chambers with physiological Krebs-Ringer solution. (B) The experimental protocol compared the isolated effects of vehicle and piperine treatment. Dynamic muscle function was assessed by performing force-velocity (FV) tests at baseline (FV1) and after the incubation (FV2) (presented in Fig. 5). The illustration in A is from Herskind 2022 (47) and Biorender.com.

Figure 3. Effects of 50 µM piperine on isometric muscle function of intact fast (extensor digitorum longus, EDL) rat skeletal muscles. Isometric twitches (2 Hz), unfused isometric tetani (50 Hz for 0.3 s), and fused isometric tetani (150 Hz for 0.2 s) were induced at regular intervals during the 60-min incubation (Incubation 1 in Fig. 2B). We show exemplary force traces from twitch, unfused tetani, and fused tetani at the start (0 min) and end (60 min) of incubation for one EDL muscle per treatment.

Figure 4. Effects of 50 µM piperine on isometric muscle function of intact slow (soleus) rat skeletal muscles. Isometric (A) twitches (2 Hz), (B) unfused isometric tetani (20 Hz for 2 s), and (C) fused isometric tetani (80 Hz for 2s) were induced at regular intervals during the 60-min incubation (Incubation 1 in Fig. 2B). We show exemplary force traces from twitch, unfused tetani, and fused tetani at the start (0 min) and end (60 min) of incubation for one soleus muscle per treatment.

Figure 5. Effects of thick-filament activation by piperine on low- and high-frequency dynamic muscle function of fast-twitch (extensor digitorum longus, EDL) and slow-twitch (soleus) skeletal muscles. (A) Exemplary contractions (n = 1 EDL muscle) used to construct force-velocity (FV) and power curves (see Fig. S2 for all contraction types). (B and C) Baseline low- and high-frequency EDL and soleus FV and power curves, respectively (mean with shades showing SEM; n = 6 muscles of each type). (D and E) Curves on the left show low-frequency EDL (60 Hz) and soleus (20 Hz) FV and power curves after contralateral piperine and vehicle treatments. Curves are normalized to baseline and show group means with shades showing SEM. Bars on the right show corresponding baseline-normalized Hill-equation estimates of: maximal unloaded shortening velocity (V_{max}), curvature of the FV curve (a/F_o, which is inversely related to curvature), and maximal power output (P_{max}) as mean ± SEM. Curve fitting is detailed in Materials and Methods. (F and G) Curves on the left show high-frequency EDL (150 Hz) and soleus (80 Hz) FV and power curves in response to treatments, with bars in the right showing corresponding estimates of V_{max}, a/F_o, and P_{max}. Circles and connecting lines represent the values of individual muscles and their contralateral pairings, respectively. P-values are from repeated measures ANOVAs (significance level: $P < 0.05$) comparing changes from baseline for piperine and vehicle. For EDL, n = 5 for piperine treatment and n = 6 for vehicle treatment. For soleus muscles, n = 6 for each treatment.

Figure 6. Effects of thick-filament activation by piperine on the overall actomyosin crossbridge cycling rate of intact fast-twitch (extensor digitorum longus, EDL) and slow-twitch (soleus) skeletal muscles. As a proxy measure of the overall actomyosin crossbridge cycling rate, we determined the rate constant of isometric tension redevelopment (K_{tr}) every 15th minute (detailed in the Materials and Methods of the SI Appendix and Table S6). (A) Exemplary force trace from an EDL muscle in response to the modified protocol from Kristensen et al. 2019 (42). (B) The insert

shows the final part of the fused tetani, the unloaded shortening, the restretch, and the force redevelopment, where K_{tr} is estimated by curve-fitting (red and dotted section). (C and D) Show the effects of 60 min of piperine and vehicle treatment on K_{tr} normalized to the values at 0 min in EDL and soleus muscles, respectively. The P-value indicates the significance of the increase relative to baseline in piperine compared to vehicle treatment using 2-way ANOVAs with Tukey's correction (statistical findings are detailed in Table S6). Mean r^2 ± SD for K_{tr} curve-fit: EDL 0.94 ± 0.05 (n = 7 pairs); soleus 0.97 ± 0.01 (n = 4 pairs). Data on the figure are shown as group means ± SEM. Circles and connecting lines represent the values of individual muscles and their contralateral pairings, respectively.

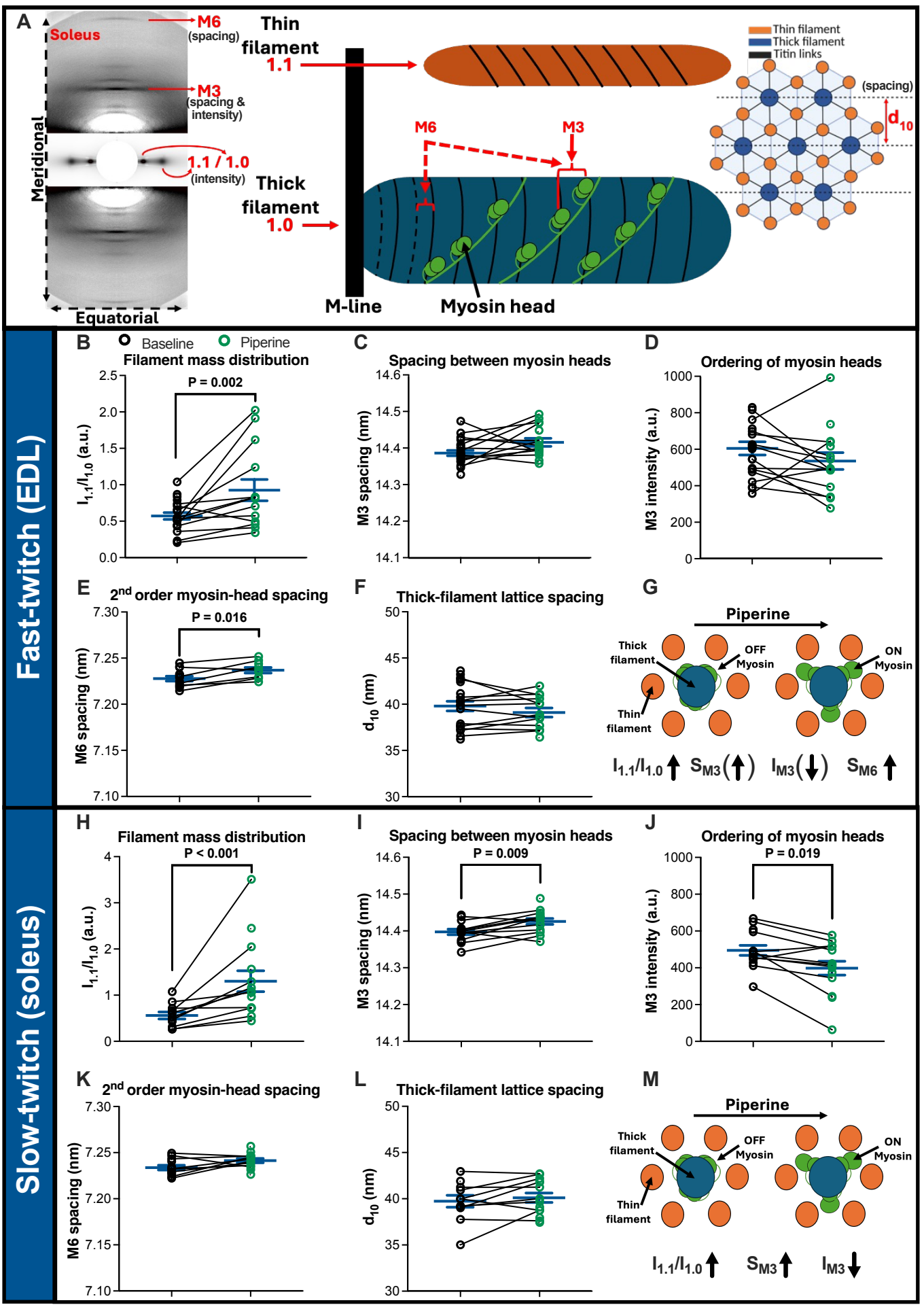
A
Soleus
M6
(spacing)
M3
(spacing & intensity)
1.1 / 1.0
(intensity)
Meridional
Equatorial
Thin filament
1.1
Thick filament
1.0
M6
M3
M-line
Myosin head
Thin filament
Thick filament
Titin links
(spacing)
d10
Fast-twitch (EDL)
B
Baseline
Piperine
Filament mass distribution
P = 0.002
I1.1/I1.0 (a.u.)
C
Spacing between myosin heads
M3 spacing (nm)
D
Ordering of myosin heads
M3 intensity (a.u.)
E
2nd order myosin-head spacing
P = 0.016
M6 spacing (nm)
F
Thick-filament lattice spacing
d10 (nm)
G
Piperine
Thick filament
OFF Myosin
ON Myosin
Thin filament
I1.1/I1.0 SM3 IM3 SM6
Slow-twitch (soleus)
H
Filament mass distribution
P < 0.001
I1.1/I1.0 (a.u.)
I
Spacing between myosin heads
P = 0.009
M3 spacing (nm)
J
Ordering of myosin heads
P = 0.019
M3 intensity (a.u.)
K
2nd order myosin-head spacing
M6 spacing (nm)
L
Thick-filament lattice spacing
d10 (nm)
M
Piperine
Thick filament
OFF Myosin
ON Myosin
Thin filament
I1.1/I1.0 SM3 IM3

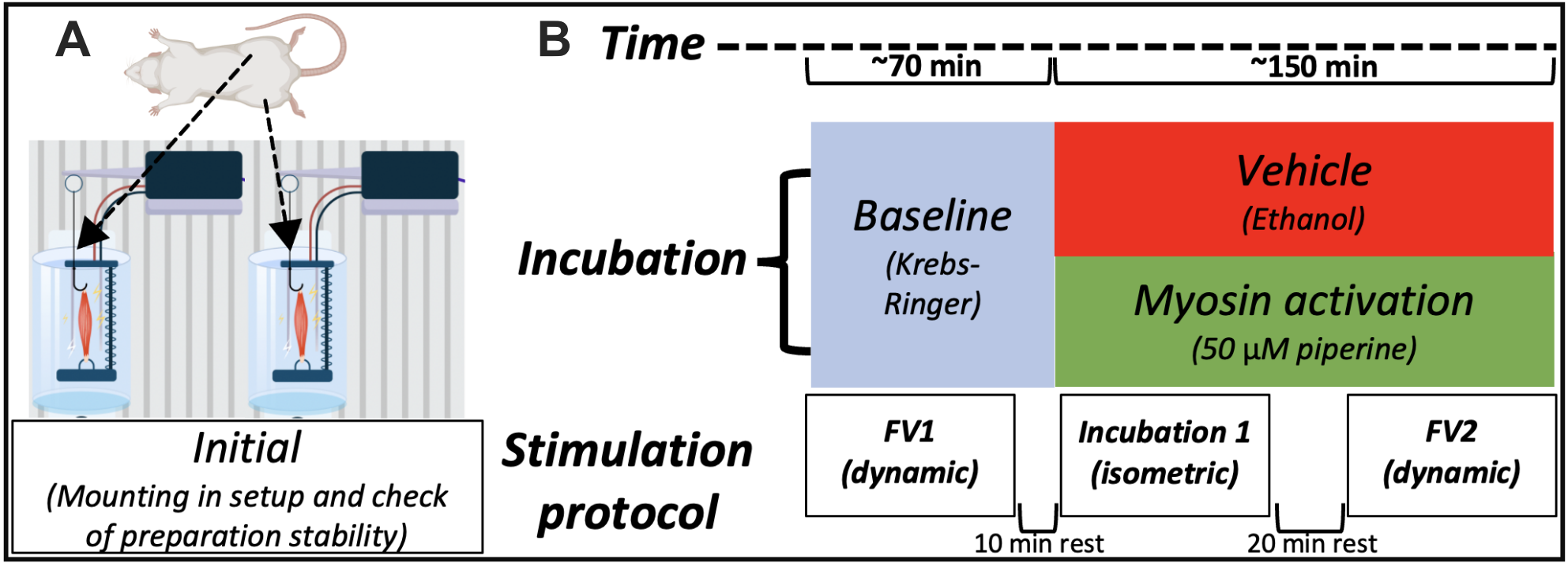
A
B
Time
~70 min
~150 min
Incubation
Baseline
(Krebs-Ringer)
Vehicle
(Ethanol)
Myosin activation
(50 µM piperine)
Initial
(Mounting in setup and check of preparation stability)
Stimulation protocol
FV1
(dynamic)
Incubation 1
(isometric)
FV2
(dynamic)
10 min rest
20 min rest

Fast-twitch (EDL)

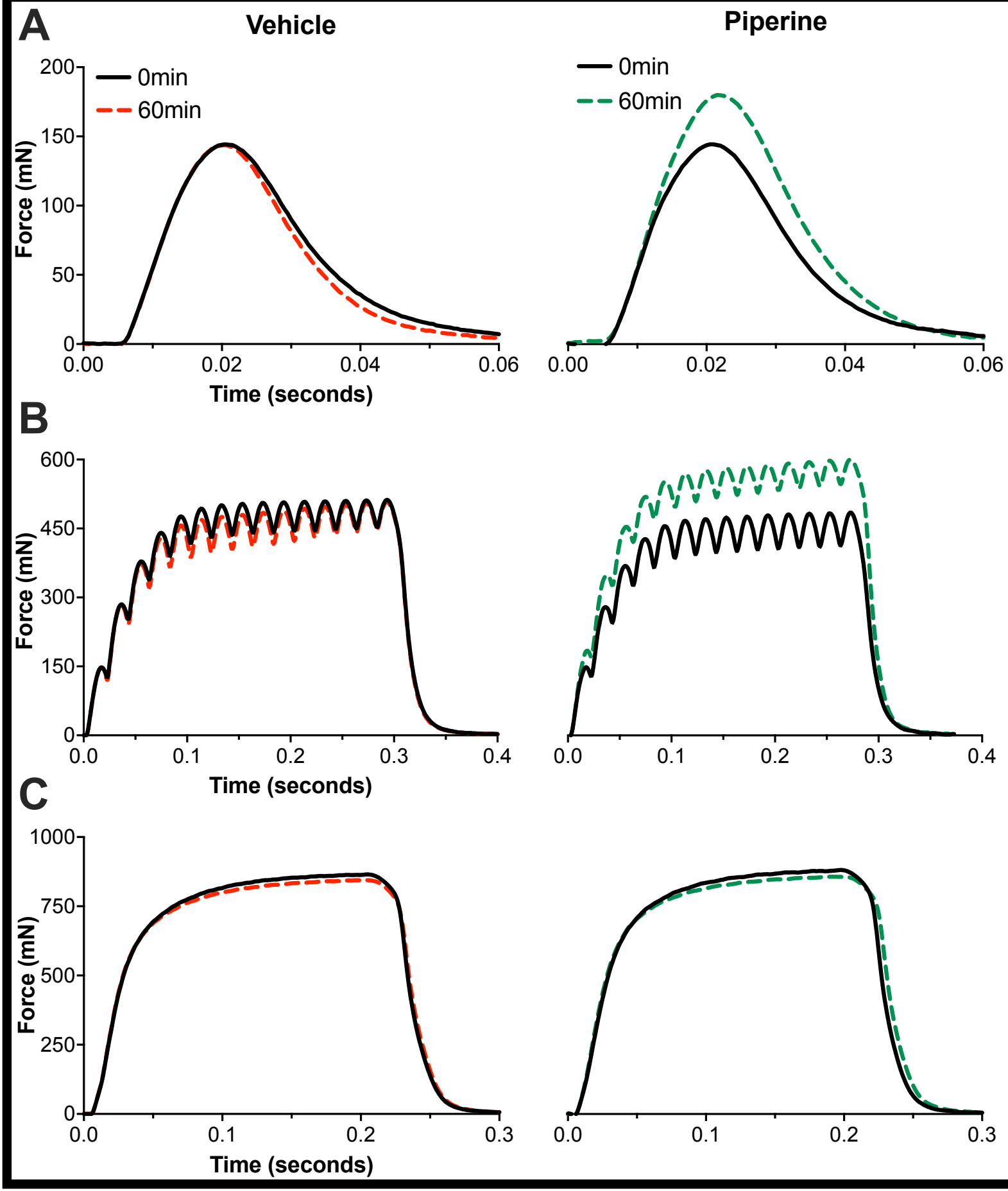

Slow-twitch (soleus)

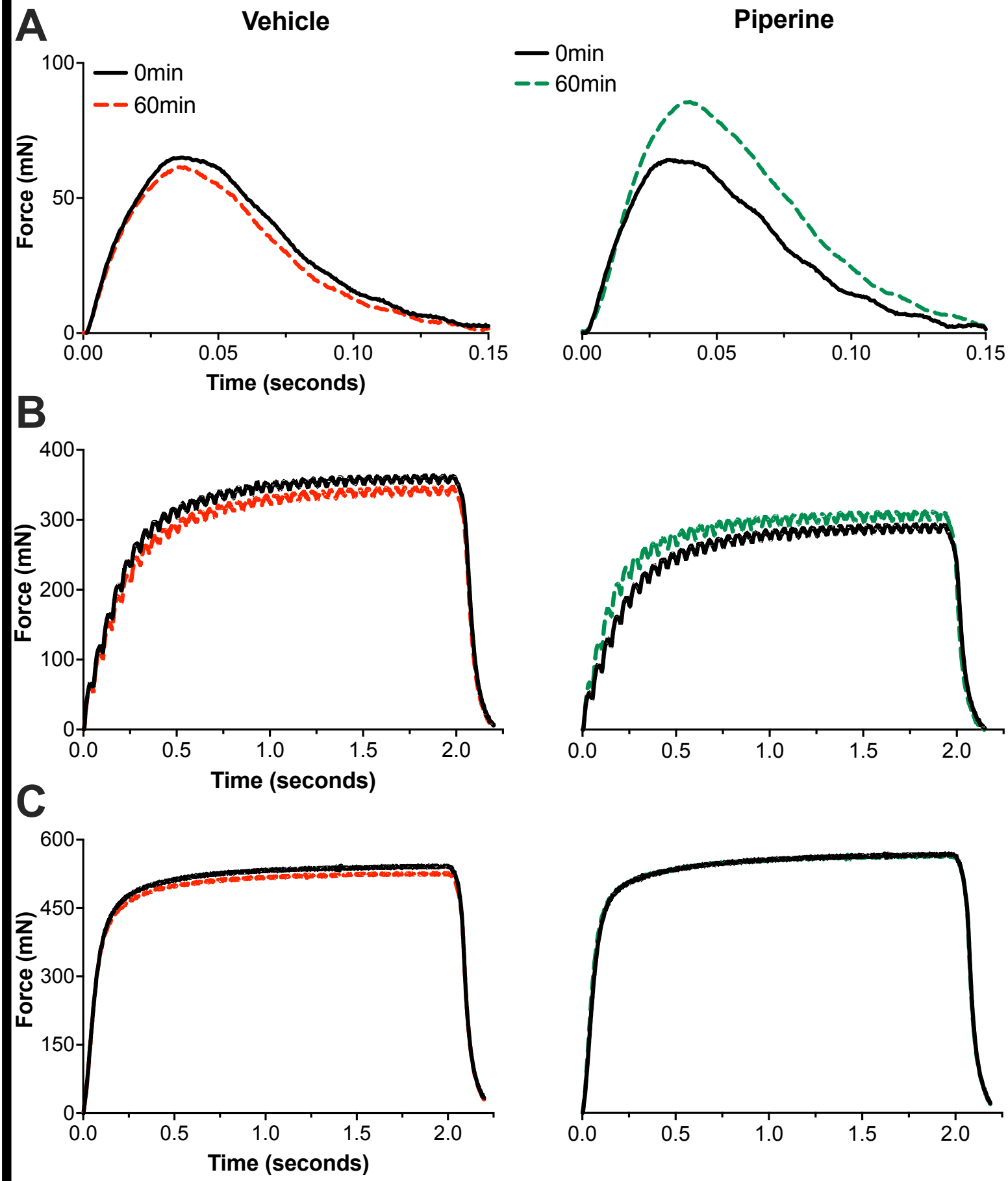

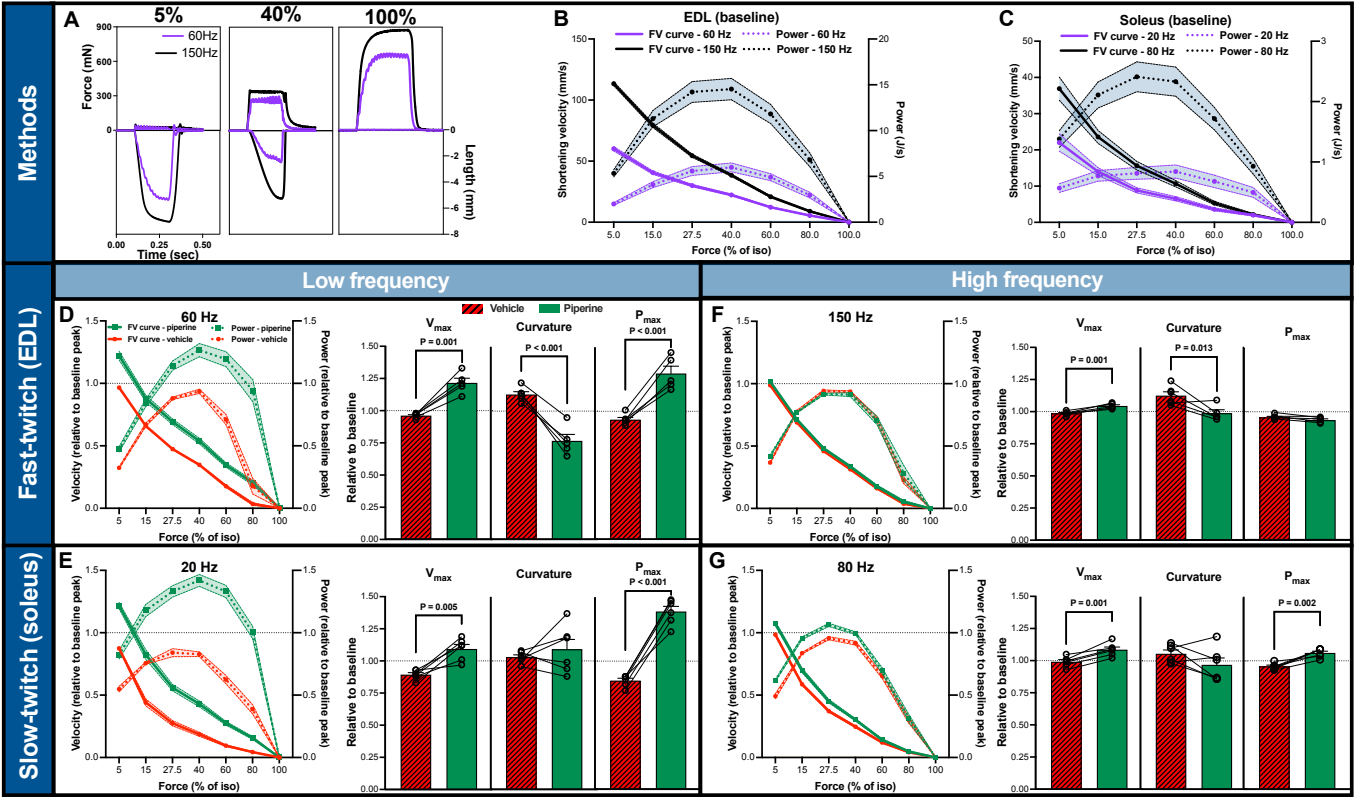
Methods
A
5%
40%
100%
60Hz
150Hz
Force (mN)
Time (sec)
Length (mm)
B
EDL (baseline)
FV curve - 60 Hz
FV curve - 150 Hz
Power - 60 Hz
Power - 150 Hz
Shortening velocity (mm/s)
Power (J/s)
Force (% of iso)
C
Soleus (baseline)
FV curve - 20 Hz
FV curve - 80 Hz
Power - 20 Hz
Power - 80 Hz
Shortening velocity (mm/s)
Power (J/s)
Force (% of iso)
Fast-twitch (EDL)
Low frequency
High frequency
D
60 Hz
FV curve - piperine
FV curve - vehicle
Power - piperine
Power - vehicle
Velocity (relative to baseline peak)
Power (relative to baseline peak)
Force (% of iso)
Vehicle
Piperine
Vmax
Curvature
Pmax
P = 0.001
P < 0.001
P < 0.001
Relative to baseline
F
150 Hz
P = 0.001
P = 0.013
E
20 Hz
P = 0.005
P < 0.001
Slow-twitch (soleus)
G
80 Hz
P = 0.001
P = 0.002

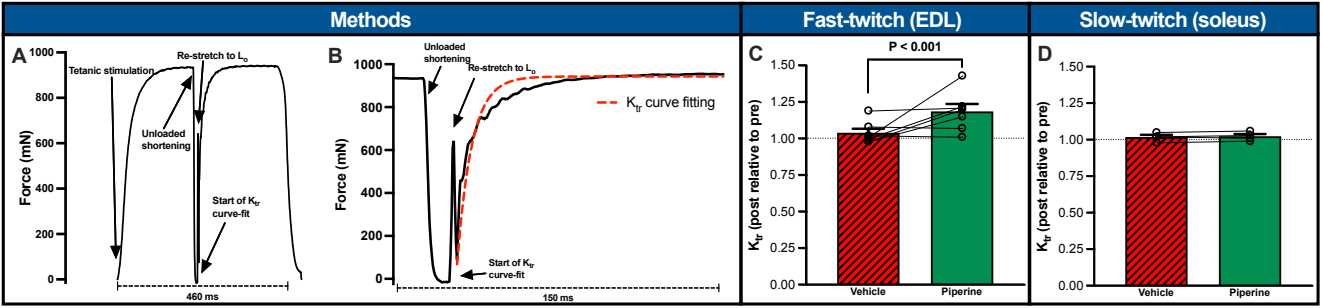
Methods
Fast-twitch (EDL)
Slow-twitch (soleus)
A
Tetanic stimulation
Re-stretch to L_o
Unloaded shortening
Start of K_{tr} curve-fit
Force (mN)
460 ms
B
Unloaded shortening
Re-stretch to L_o
K_{tr} curve fitting
Start of K_{tr} curve-fit
Force (mN)
150 ms
C
P < 0.001
K_{tr} (post relative to pre)
Vehicle
Piperine
D
K_{tr} (post relative to pre)
Vehicle
Piperine